

The OPS-SAT benchmark for detecting anomalies in satellite telemetry

Bogdan Ruszczak^{1,3,*}, Krzysztof Kotowski³, David Evans⁴, and Jakub Nalepa^{2,3}

¹Faculty of Electrical Engineering, Automatic Control and Informatics, Department of Informatics, Opole University of Technology, Prószkowska Str. 76, 45-758 Opole, Poland

²Faculty of Automatic Control, Electronics and Computer Science, Department of Algorithmics and Software, Silesian University of Technology, Akademicka Str. 16, 44-100 Gliwice, Poland

³KP Labs, Bojkowska Str. 37J, 44-100 Gliwice, Poland

⁴European Space Agency/ESOC, Robert-Bosch-Str. 5, 64293 Darmstadt, Germany

*corresponding author(s): Bogdan Ruszczak (b.ruszczak@po.edu.pl)

ABSTRACT

Detecting anomalous events in satellite telemetry is a critical task in space operations. This task, however, is extremely time-consuming, error-prone and human dependent, thus automated data-driven anomaly detection algorithms have been emerging at a steady pace. However, there are no publicly available datasets of real satellite telemetry accompanied with the ground-truth annotations that could be used to train and verify anomaly detection supervised models. In this article, we address this research gap and introduce the AI-ready benchmark dataset (OPSSAT-AD) containing the telemetry data acquired on board OPS-SAT—a CubeSat mission which has been operated by the European Space Agency which has come to an end during the night of 22–23 May 2024 (CEST). The dataset is accompanied with the baseline results obtained using 30 supervised and unsupervised classic and deep machine learning algorithms for anomaly detection. They were trained and validated using the training-test dataset split introduced in this work, and we present a suggested set of quality metrics which should be always calculated to confront the new algorithms for anomaly detection while exploiting OPSSAT-AD. We believe that this work may become an important step toward building a fair, reproducible and objective validation procedure that can be used to quantify the capabilities of the emerging anomaly detection techniques in an unbiased and fully transparent way.

Background & Summary

The anomaly detection (AD) domain encompasses a diverse array of methodologies for the identification of anomalous patterns in data of various modalities. These approaches can be applied to a multitude of data types, including images, text, and time series data, among others. However, the development and evaluation of real-world anomaly detection applications are dependent on the availability of real-world data. Currently, there is a considerable number of datasets available for a wide range of scenarios¹, but the satellite telemetry data for AD is an extremely underrepresented category in this catalogue. This kind of data is difficult and costly to obtain, often confidential, and requires expert knowledge to annotate properly. The only two widely accessible and used collections of this type include the NASA Soil Moisture Active Passive (SMAP) and Mars Science Laboratory (MSL) datasets². They offer short fragments of signals and related commands from 55 and 27 telemetry parameters, respectively, with a total of 105 annotated anomalies. However, the recent consensus in the community is that they should not be used for time series AD benchmarking due to their unrealistic anomaly density, many trivial anomalies, mislabelled ground truth, distributional shifts, and a lack of meaningful correlation between commands and channels³⁻⁵. Other well-known satellite telemetry datasets, such as Mars Express⁶ or NASA WebTCAD⁷, do not contain annotations of anomalous events. There is an ongoing activity to publish a large-scale AD dataset by European Space Agency (ESA) solving all the mentioned issues^{8,9}, but it will primarily address the needs of large-scale, complex and relatively stable missions.

The dataset introduced in this article, dubbed OPSSAT-AD, is fundamentally different from those available in the literature, as it tackles a very specific ESA OPS-SAT mission—a CubeSat flying laboratory, for which we might expect a noticeable number of abnormal events¹⁰. The raw telemetry from OPS-SAT is characterized by many data gaps, artifacts, sampling frequency changes, and signal amplitude variations. The dataset was collectively curated by space operations engineers and machine learning experts to make it useful for building and validating data-driven anomaly detection techniques. It includes a selection and the corresponding ground-truth annotation of 2123 short single-channel satellite telemetry fragments (univariate time series) captured within 9 telemetry channels. Due to the underlying nature of the OPS-SAT mission, anomalous fragments account for 20% of the dataset. Such fragments contain raw data with many aforementioned real-life challenges, and they differ

in their length and sampling frequency. For each telemetry fragment, the dataset also contains a set of 18 handcrafted features used in the actual machine learning AD algorithm validated on board OPS-SAT¹¹. These features are exploited in this article to benchmark 30 other supervised and unsupervised machine learning algorithms for anomaly detection. All of them were trained on 1494 and tested on 529 telemetry segments, and assessed using 7 metrics suggested for quantifying the operational capabilities of anomaly detection algorithms—this training-test dataset split is included in our benchmark as well.

Overall, the benchmark (including the dataset, training-test dataset split, suggested quality metrics, and our baseline results) introduced in this paper shall help the community to create and compare their approaches to detecting anomalies in real-life satellite telemetry in a fair and unbiased way. Therefore, we also address the reproducibility crisis currently observed in the (not only) machine learning community¹². While the OPS-SAT spacecraft completed its atmospheric reentry at the end of May 2024, its successor—OPS-SAT VOLT—is going to be launched in late 2025 and will make a great opportunity to validate the algorithms developed based on our benchmark in the wild after deploying them on-board an operational satellite.

Methods

Data acquisition and annotation

The telemetry data delivered¹³ in this paper was acquired from the ESA OPS-SAT satellite (Figure 1). It is a small 3U, where 1U=10 cm³) CubeSat launched in December 2019 with the primary objective of being a technological demonstrator for in-orbit data processing. It finished its mission with the atmospheric reentry on 22 May 2024, but it generated lots of useful data during more than 4 years of its operations, including satellite imagery¹⁴ and telemetry¹¹.

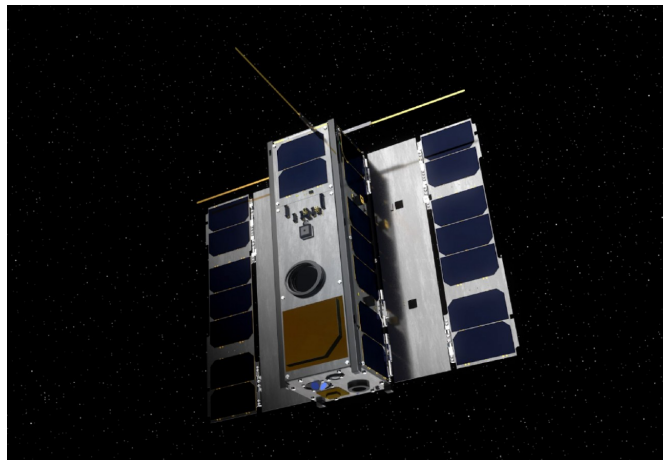


Figure 1. The ESA OPS-SAT frontal view. Image credits: European Space Agency.

OPS-SAT offered a unique opportunity for researchers to run their experiments and algorithms in orbit. While these experiments were carried out, all telemetry data was simultaneously collected and recorded in the ESA archive. The archive was monitored for potential anomalies to ensure the mission’s stable and uninterrupted operation. Our dataset consists of telemetry fragments recommended by the OPS-SAT operation engineers as the most “interesting” (according to their subjective assessment) for anomaly detection. The actual data collection process was carried out using the data exchange platform WebMUST¹⁵ used in the European Space Operations Centre (ESOC). This platform is restricted to the authorized ESA partners only, but the data included in our dataset package does not have to be requested through it, and thus is made publicly available.

The online OXI tool for visualization and annotation of satellite telemetry (<https://oxi.kplabs.pl/>)¹⁶ was used to enable a collaborative labeling process of the dataset. Using this application, domain experts were able to manually extract and annotate telemetry segments representing periods of nominal and anomalous operation. The initial selection of anomalies was provided by 3 ESA spacecraft operations engineers and further curated by 2 machine learning experts (with more than 10 years of experience each). The curated annotations were finally reviewed by the three spacecraft operations engineers. The detailed satellite telemetry annotation process, together with the visual artefacts generated throughout it, are discussed in^{11,17,18}.

Feature extraction

Due to the characteristics of satellite telemetry, the segments of raw data selected by the domain experts have varying lengths and sampling frequency. As such, they could not be handled by most machine learning algorithms without performing an additional preprocessing or feature extraction. Thus, 18 handcrafted features were designed for the task of anomaly detection¹¹—they

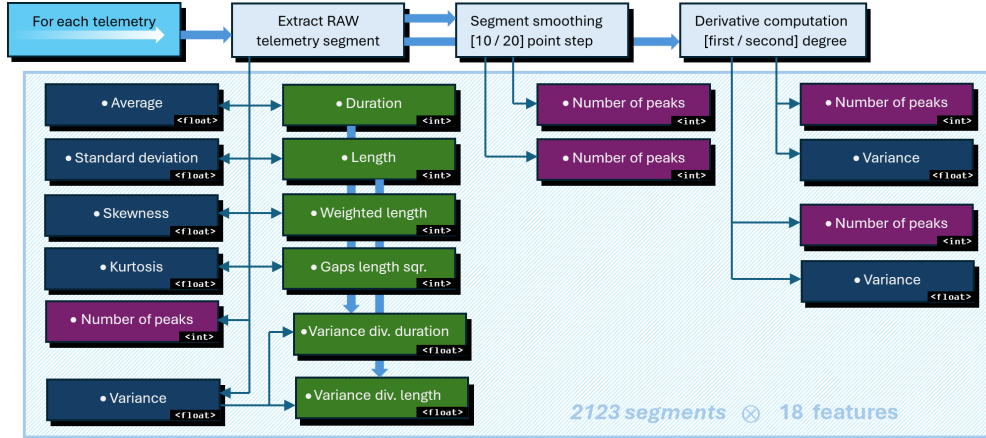


Figure 2. The features extracted for each segment, with the corresponding data type. The meaning of the colors: dark blue for popular statistics, violet for peak counters for various converted segments, and green for the length or duration-related features.

were calculated separately for each segment, and they are included in our benchmark. An algorithm operating on such features was already validated in our previous work focusing on the application of data-driven anomaly detection on board OPS-SAT¹¹.

The features extracted for each telemetry segment are presented in Figure 2. They are divided into three groups:

- **12 features extracted from raw segments**, including basic statistics, such as the arithmetic average of the signal values, their standard deviation, skewness, kurtosis and variance ($\langle mean \rangle$, $\langle std \rangle$, $\langle skew \rangle$, $\langle kurtosis \rangle$, and $\langle var \rangle$), but also the number of peaks (of the minimum of 10% prominence, with a peak prominence measuring how much a peak “stands out” in relation to the signal, while considering its height and location: $\langle n_peaks \rangle$), duration (in seconds: $\langle duration \rangle$) and the length (in the number of telemetry points: $\langle len \rangle$), the weighted length (weighted by sampling: $\langle len_weighted \rangle$), the gaps’ length (the squared number of missing data points: $\langle gaps_squared \rangle$), and the weighted variance (weighted by the duration and by the length: $\langle var_div_duration \rangle$, $\langle var_div_len \rangle$).
- **2 features extracted from the smoothed segments (using the uniform interpolation¹⁹)**, including the number of peaks (extracted using the 10 and 20 points smoothing steps: $\langle smooth10_n_peaks \rangle$, $\langle smooth20_n_peak \rangle$).
- **4 features extracted from the first and the second derivatives of the segment**, including the number of peaks and variance ($\langle diff_peaks \rangle$, $\langle diff2_peaks \rangle$, $\langle diff_var \rangle$, $\langle diff2_var \rangle$).

Employing the duration, the length and the gaps’ length features should allow the algorithms to easily capture some “obvious” abnormalities in the telemetry data. This intuitively could lead to promote some less computationally demanding AD methods suitable for on-board applications. The proposed set of features serves as an example and may be easily expanded (or replaced) by the community by (i) designing new feature extractors (potentially followed by feature selectors), (ii) using other well-established feature sets²⁰ or (iii) benefiting from the automated feature learning²¹.

Benchmarking procedure

We provide a procedure that should be followed to confront the AD algorithms over our dataset. The entire dataset of 2123 telemetry segments is split into the training (\mathcal{T}) and test (Ψ) sets (Table 1), forming an AI-ready dataset. To extract these subsets, we performed the stratified random sampling to maintain the original percentage of anomalies in both \mathcal{T} and Ψ .

Table 1. The number of telemetry segments included in the training (\mathcal{T}) and test (Ψ) sets.

Class	Training set (\mathcal{T})	Test set (Ψ)	Total
Nominal	1273	416	1689
Anomalous	321	113	434
Sum	1494	529	2123

The benchmarking procedure can be summarized by the following steps:

1. Load the dataset from the `dataset.csv` file.

2. Split the dataset into \mathbf{T} and Ψ according to the $\langle train \rangle$ attribute included in this file.
3. [Optionally] Preprocess the datasets using e.g., data normalization, additional feature extraction, feature selection and other steps directly related to the AD algorithm which undergoes the benchmarking process.
4. [Optionally] Train a machine learning model over \mathbf{T} .
5. Quantify the algorithm’s performance over Ψ using the metrics discussed in the next section.

Quality metrics

The following metrics should always be calculated over the test set Ψ while confronting the AD algorithms (both supervised and unsupervised) over the dataset OPSSAT-AD introduced in this work:

- **Accuracy:** $(TP + TN) / (TP + TN + FP + FN)$,
- **Precision:** $TP / (TP + FP)$,
- **Recall:** $TP / (TP + FN)$,
- **F_1 score:** $(2 \cdot \text{precision} \cdot \text{recall}) / (\text{precision} + \text{recall})$,
- **Matthews’ Correlation Coefficient (MCC)²²:** $(TP \cdot TN - FP \cdot FN) / \sqrt{(TP + FP) \cdot (TP + FN) \cdot (TN + FP) \cdot (TN + FN)}$,
- **Area under the receiver operating characteristic curve (AUC_{ROC}),**
- **Area under the precision-recall curve (AUC_{PR}),**

where TP , TN , FP , and FN are the number of true positives (anomalous telemetry segments correctly identified as anomalies), true negatives (nominal telemetry segments correctly identified as nominal), false positives (nominal telemetry segments incorrectly identified as anomalies), and false negatives (anomalous telemetry segments incorrectly identified as nominal). All metrics should be maximized (\uparrow), with one indicating the best score (MCC ranges from -1 to 1 , other metrics from 0 to 1).

The baseline: anomaly detection algorithms

Although there are ground-truth AD datasets that may be used to train supervised models for this task, they are extremely limited and, by definition, they cannot capture a representative set of anomalies (otherwise such “anomalies” would not be “anomalies” any longer). In practice, while building data-driven AD algorithms for satellite telemetry, practitioners may not be able to access real-life ground-truth data, hence unsupervised methods have been gaining research attention. Here, we establish a set of baseline results obtained using 30 AD methods, including both supervised and unsupervised algorithms (Table 2).

For all those algorithms, implemented in the PyOD framework⁵¹ (<https://pyod.readthedocs.io/en/latest/>), the default parameters (suggested by the authors of these techniques) are used, with the anomaly contamination factor set to 0.2 , according to the anomaly distribution observed in \mathbf{T} . To ensure reproducibility, we provide a Jupyter Notebook showing how to execute an example AD algorithm, in a both supervised and unsupervised training regime (*modeling_examples.ipynb*).

Dataset Layout

The dataset¹³ is built of 9 source telemetry channels that were selected by the space operations engineers. They include 3 magnetometer telemetry channels: I_B_FB_MM_0 (CADC0872), I_B_FB_MM_1 (CADC0873), I_B_FB_MM_2 (CADC0874), and 6 photo diode (PD) channels: I_PD1_THETA (CADC0884), I_PD2_THETA (CADC0886), I_PD3_THETA (CADC0888), I_PD4_THETA (CADC0890), I_PD5_THETA (CADC0892), I_PD6_THETA (CADC0894). Here, the names correspond to the source names from the WebMUST repository and the OPS-SAT telemetry channel names (in brackets). The layout of the dataset is summarized in Figure 3—it includes both the raw files, as well as the extracted features in a tabular form.

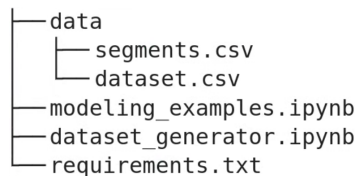


Figure 3. The layout of the OPS-SAT benchmark for anomaly detection.

Abbreviation	Year	Algorithm
<i>Supervised algorithms</i>		
Linear+L2 ²³	2006	Linear classifier with L_2 regularization
LR ²⁴	2008	Logistic regression
AdaBoost ²⁵	2009	Adaptive Boosting
LSVC ²⁶	2013	Support Vector Classifier with the squared hinge linear loss
XGBOD ²⁷	2018	Extreme Gradient Boosting Outlier Detection
FCNN ²⁸	2019	Fully Connected Neural Network with dropout and batch normalization
RF+ICCS ¹¹	2023	Random Forest based model with segment augmentation
<i>Unsupervised algorithms</i>		
PCA ^{29,30}	1996	Principal Component Analysis
LMDD ³¹	1996	Linear Method for Deviation Detection
COF ³²	2002	Connectivity-based Outlier Factor
KNN ³³	2002	K-Nearest Neighbors
CBLOF ³⁴	2003	Cluster-Based Local Outlier Factor
ABOD ³⁵	2008	Angle-based Outlier Detector
IForest ³⁶	2008	Isolation Forest
SOD ³⁷	2009	Outlier Detection in Axis-Parallel Subspaces of High Dimensional Data
SOS ³⁸	2012	Stochastic Outlier Selection
VAE ³⁹	2013	Variational Autoencoder
OCSVM ⁴⁰	2016	One-Class Support Vector Machine with a polynomial kernel
LODA ⁴¹	2016	Lightweight On-line Detector of Anomalies
GMM ³⁰	2017	Gaussian Mixture Model
AnoGAN ⁴²	2017	Generative Adversarial Networks for AD
DeepSVDD ⁴³	2018	Deep one-class classification
ALAD ⁴⁴	2018	Generative Adversarial Networks for AD
INNE ⁴⁵	2018	Isolation-based Anomaly Detection Using Nearest-Neighbor Ensembles
SO-GAAL ⁴⁶	2020	Single-objective Generative Adversarial Active Learning
MO-GAAL ⁴⁶	2020	Multi-objective Generative Adversarial Active Learning
COPOD ⁴⁷	2020	Copula-based outlier detection
ECOD ⁴⁸	2022	Empirical Cumulative Distribution Functions
LUNAR ⁴⁹	2022	Unified Local Outlier Detection with Graph Neural Networks
DIF ⁵⁰	2023	Deep Isolation Forest

Table 2. Anomaly detection methods investigated in this study.

Raw telemetry data

In Figure 4, we visualize selected characteristics of the acquired telemetry signals, effectively showing real-world challenges concerned with telemetry data acquired in the wild (e.g., missing readouts, different sampling frequencies). Such segments for all the aforementioned telemetry channels and their selected parts are included in the `data/segments.csv` file. It contains the attributes that identify the registration time: $\langle timestamp \rangle$ (ISO date format), $\langle channel \rangle$ (the channel name), $\langle value \rangle$ (the acquired signal value), and $\langle label \rangle$ (the ground-truth annotation). Additionally, we provide the consecutive segment numbers ($\langle segment \rangle$), their sampling rate ($\langle sampling \rangle$), and the indication if they are included in \mathbf{T} ($\langle train \rangle$).

Extracted features

In the tabular version of the dataset (`data/dataset.csv`), we include the extracted features. In the Supplementary Materials, we present the distributions of all of the provided features, rendered for both \mathbf{T} and Ψ sets of our dataset (Figure 7).

Experimental Validation

In Table 3, we aggregate the results obtained using all the investigated AD algorithms. Here, we highlighted the globally best results (in bold for each quality metric), and we underlined the best results elaborated by the unsupervised algorithms, as we consider them a different category of the AD solutions. We are aware that some algorithms from PyOD should be rather trained using nominal data only (i.e., OCSVM or autoencoders) to achieve better results. As an example, the OCSVM model achieves AUC_{PR} of 0.659 and AUC_{ROC} of 0.787 in our setting, but when using only the nominal data (without abnormal segments) for

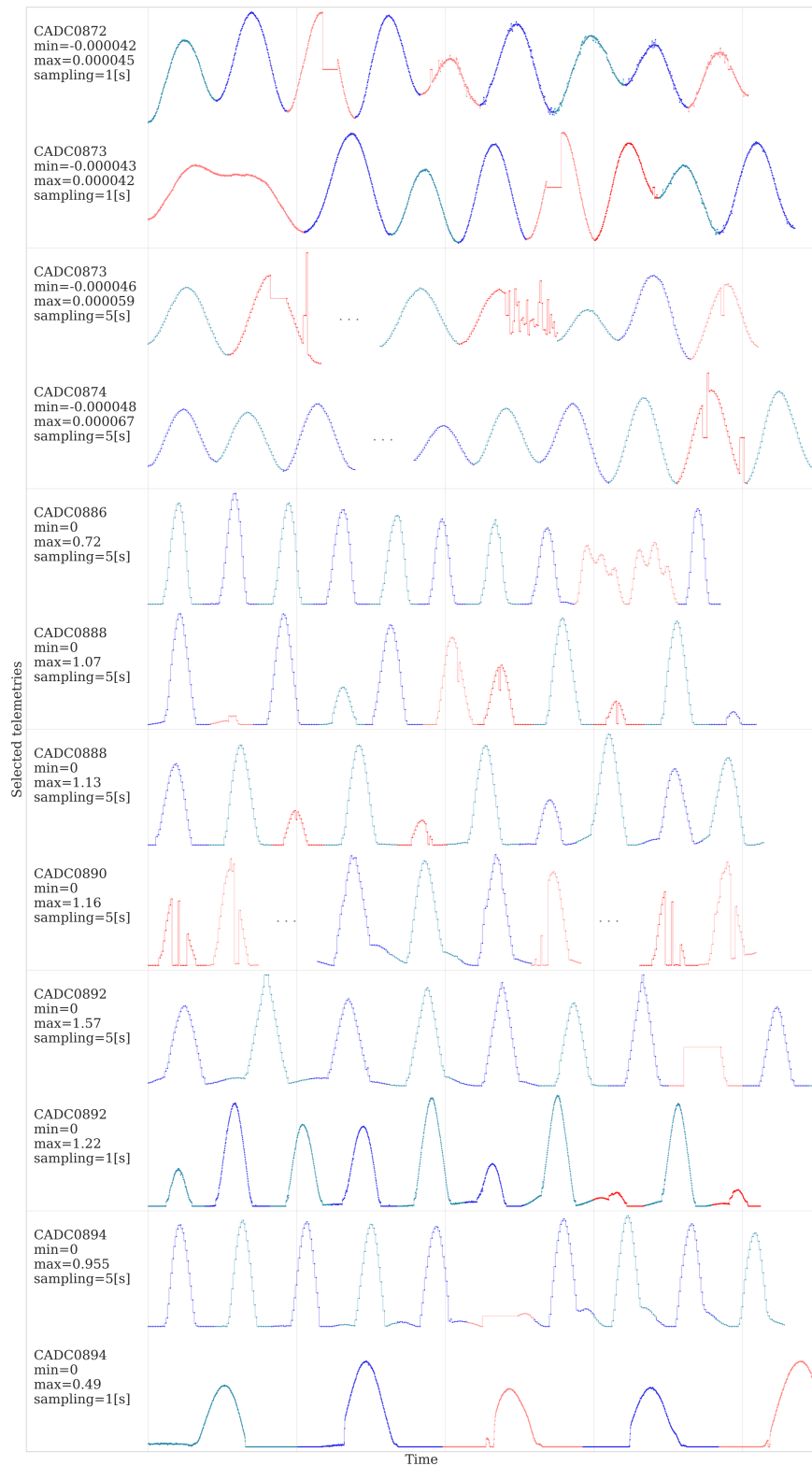


Figure 4. Selected segments from out OPS-SAT dataset. Several types of signal distortions are depicted, including peaks, deformations, noise (CADC0873), irregular periodicity (CADC0886), short (CADC0892, CADC0894) and long data gaps (CADC0874). Anomalous segments are plotted in red. For brevity, we omit the axis values, but provide data ranges and the sampling information for each channel.

training, the corresponding values are 0.762 and 0.815. However, we wanted our baseline to be consistent and to reflect a typical usage of the PyOD framework by a non-expert user. Also, the fine-tuning of those algorithms is out of the scope of this study. In Figure 5, we render the selected metrics for each model. We can indeed observe the better performance of supervised methods, as those could actively benefit from the labeled anomaly examples while building a machine learning model. In Figure 6, we also display the precision and recall quality metrics. For the fully-connected neural network, we can observe only four false positives and eight false negatives of all Ψ samples, reaching the precision of 0.963, and the recall of 0.929.

Model	AUC_{PR} (\uparrow)	AUC_{ROC} (\uparrow)	Accuracy (\uparrow)	F_1 (\uparrow)	Precision (\uparrow)	Recall (\uparrow)	MCC (\uparrow)
<i>Supervised algorithms</i>							
FCNN	0.979	0.989	0.977	0.946	0.963	0.929	0.932
XGBOD	0.975	0.992	0.966	0.918	0.944	0.894	0.897
RF+ICCS	0.963	0.985	0.955	0.883	0.978	0.805	0.862
LSVC	0.934	0.968	0.926	0.808	0.911	0.726	0.771
LR	0.931	0.969	0.924	0.800	0.920	0.708	0.764
AdaBoost	0.923	0.962	0.934	0.836	0.890	0.788	0.797
Linear+L2	0.901	0.958	0.905	0.722	0.970	0.575	0.703
<i>Unsupervised algorithms</i>							
MO-GAAL	<u>0.779</u>	<u>0.865</u>	<u>0.907</u>	<u>0.726</u>	0.985	0.575	<u>0.710</u>
AnoGAN	0.668	<u>0.756</u>	0.868	0.588	0.877	0.442	<u>0.563</u>
SO-GAAL	0.660	0.749	0.885	0.655	0.906	0.513	0.627
OCSVM	0.659	0.787	0.845	0.647	0.630	<u>0.664</u>	0.548
KNN	0.658	0.852	0.824	0.575	0.594	<u>0.558</u>	0.465
ABOD	0.644	0.843	0.832	0.582	0.620	0.549	0.479
INNE	0.643	0.806	0.847	0.646	0.638	0.655	0.549
ALAD	0.629	0.744	0.870	0.596	0.879	0.451	0.570
LMDD	0.623	0.767	0.854	0.628	0.691	0.575	0.542
SOD	0.621	0.797	0.737	0.505	0.423	0.628	0.348
COF	0.603	0.774	0.794	0.576	0.514	0.655	0.448
LODA	0.597	0.748	0.822	0.588	0.583	0.593	0.475
LUNAR	0.540	0.792	0.813	0.407	0.630	0.301	0.342
CBLOF	0.493	0.642	0.756	0.427	0.429	0.425	0.272
DIF	0.465	0.797	0.790	0.035	1.000	0.018	0.118
VAE	0.450	0.680	0.796	0.349	<u>0.547</u>	0.257	0.272
GMM	0.426	0.713	0.737	0.393	0.388	0.398	0.225
DeepSVDD	0.375	0.610	0.775	0.279	0.442	0.204	0.184
PCA	0.373	0.612	0.728	0.357	0.360	0.354	0.185
IForest	0.347	0.635	0.701	0.295	0.297	0.292	0.105
ECOD	0.340	0.637	0.720	0.345	0.345	0.345	0.167
COPOD	0.328	0.627	0.703	0.270	0.284	0.257	0.084
SOS	0.308	0.524	0.705	0.264	0.283	0.248	0.081

Table 3. The experimental results, sorted by AUC_{PR} . The globally best results for each metric are **boldfaced**, and the best among the unsupervised algorithms are underlined.

The investigation of the unsupervised algorithms reveals that some of them reach a point where they return a small set of mistakenly assessed telemetry samples. Especially the detectors built upon MO-GAAL, SO-GAAL and AnoGAN offered high precision. In terms of the number of misclassified examples, MO-GAAL obtained a better result than the supervised methods, and made one less false detection when compared to FCNN. A number of other unsupervised algorithms, however, tend to either return a large number of false negatives, or to raise many false alarms with a low number of false negatives. In the first group of such methods, we can observe DIF, ALAD, DeepSVDD, and AnoGAN, whereas e.g., COF belongs to the second group here. The usability of such algorithms would be rather limited to situations when avoiding one type of the classification error could be more practically important (e.g., to minimize the overhead induced on the space operations teams that would have to review many incorrectly raised false alarms).

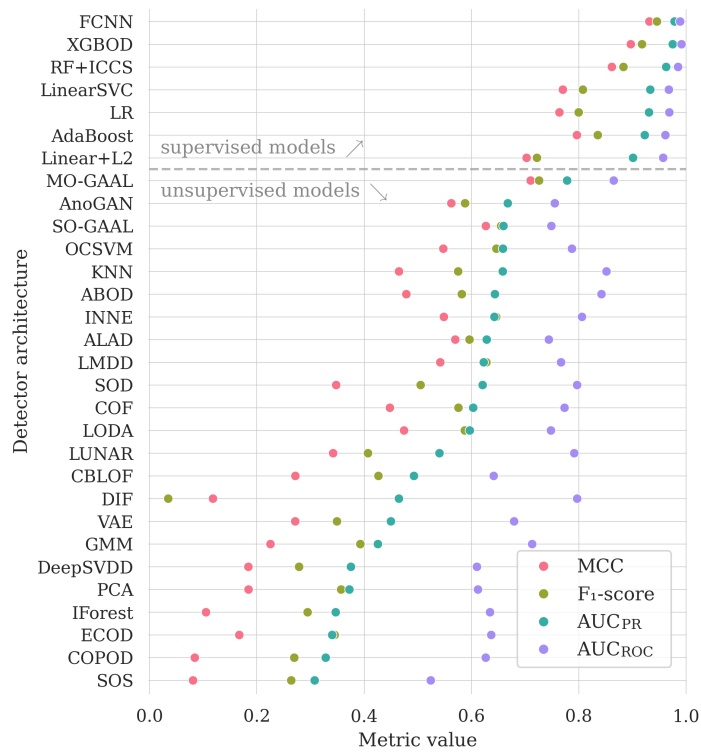


Figure 5. The results (over Ψ) obtained using the investigated machine learning models (first grouped according to their training strategy, either supervised or unsupervised, than sorted by F_1).

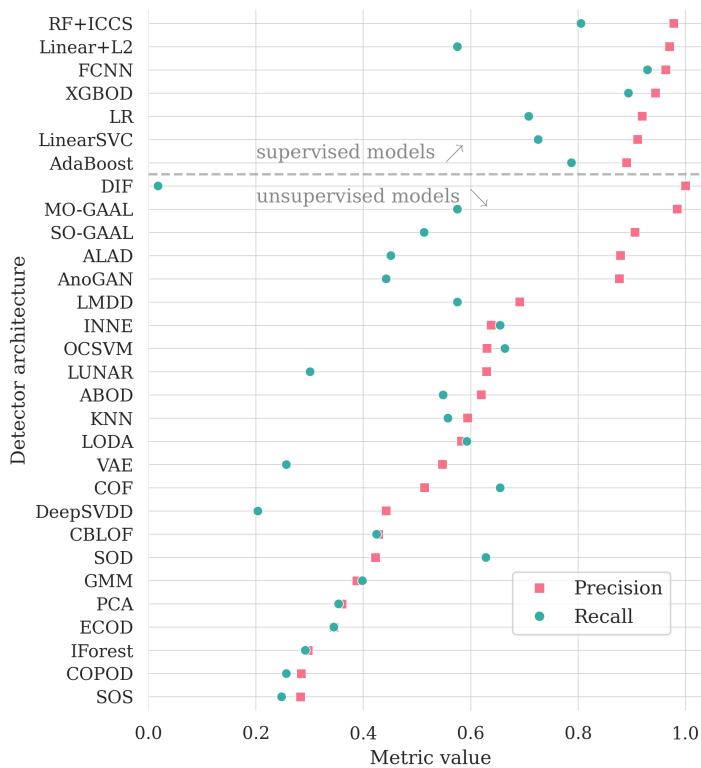


Figure 6. Precision and recall metrics (over Ψ) obtained using the investigated algorithms. Models are sorted according to the number of misclassified telemetry segments, with the best-performing one rendered on top of the graph.

Usage Notes

The dataset¹³ contains the data in two different forms: a set of the original telemetry segments and a corresponding set of handcrafted features, both with anomaly labels. Both collections are also encoded in the popular, easy-to-handle CSV format and are ready to use with various machine learning models (thus, they can be considered AI-ready). All the algorithms were implemented in Python using PyOD⁵² 1.1.2, TensorFlow⁵³ 2.15, and PyTorch⁵⁴ 2.1.2. Additionally, we used NumPy⁵⁵ 1.26.2 and Pandas⁵⁶ 2.1.14 for data preparation, Seaborn⁵⁷ 0.13.0 for the visualizations, as well as OXI¹⁶ for the initial data analysis and labeling processes. Finally, our benchmark is accompanied with a Jupyter Notebook, containing an example experiment (`modeling_examples.ipynb`), in order to ensure the experimental reproducibility.

Code Availability

The code for working with the OPS-SAT benchmark, including the functionalities used to prepare the numerical results, figures, and tables for this article, is available through the following GitHub repository: <https://github.com/kplabs-pl/OPS-SAT-AD> under the MIT license.

References

1. Pang, G., Shen, C., Cao, L. & Hengel, A. V. D. Deep learning for anomaly detection: A review. *ACM Comput. Surv. (CSUR)* **54**, 1–38 (2021).
2. Hundman, K., Constantinou, V., Laporte, C., Colwell, I. & Soderstrom, T. Detecting Spacecraft Anomalies Using LSTMs and Nonparametric Dynamic Thresholding. In *Proceedings of the 24th ACM SIGKDD International Conference on Knowledge Discovery & Data Mining, KDD '18*, 387–395, <https://doi.org/10.1145/3219819.3219845> (Association for Computing Machinery, New York, NY, USA, 2018).
3. Wu, R. & Keogh, E. Current Time Series Anomaly Detection Benchmarks are Flawed and are Creating the Illusion of Progress. *IEEE Transactions on Knowl. Data Eng.* **35**, 2421–2429, <https://doi.org/10.1109/TKDE.2021.3112126> (2023).
4. Wagner, D. *et al.* TimeSeAD: Benchmarking Deep Multivariate Time-Series Anomaly Detection. *Transactions on Mach. Learn. Res.* (2023).
5. Amin Maleki Sadr, M., Zhu, Y. & Hu, P. An Anomaly Detection Method for Satellites Using Monte Carlo Dropout. *IEEE Transactions on Aerosp. Electron. Syst.* **59**, 2044–2052, <https://doi.org/10.1109/TAES.2022.3206257> (2023). Conference Name: IEEE Transactions on Aerospace and Electronic Systems.
6. Petković, M. *et al.* Machine-learning ready data on the thermal power consumption of the mars express spacecraft. *Sci. Data* **9**, 229, <https://doi.org/10.1038/s41597-022-01336-z> (2022).
7. Sanchez, F. *et al.* WebTCAD: A Tool for Ad-hoc Visualization and Analysis of Telemetry Data for Multiple Missions. In *2018 SpaceOps Conference*, <https://doi.org/10.2514/6.2018-2616> (American Institute of Aeronautics and Astronautics, Marseille, France, 2018).
8. Kotowski, K., Haskamp, C., Ruszczak, B., Andrzejewski, J. & Nalepa, J. Annotating large satellite telemetry dataset for ESA international AI anomaly detection benchmark. In Soille, P., Lumnitz, S. & Albani, S. (eds.) *Proceedings of the 2023 conference on Big Data from Space (BiDS'23) – From foresight to impact – 6-9 November 2023, Austrian Center, Vienna, 2023*, 341–344, <https://doi.org/10.2760/46796> (Publications Office of the European Union, Luxembourg, 2023).
9. Kotowski, K. *et al.* European Space Agency Benchmark for Anomaly Detection in Satellite Telemetry (2024). ArXiv:2406.17826 [cs].
10. Evans, D. J. OPS-SAT: FDIR Design on a Mission that Expects Bugs - and Lots of Them. In *SpaceOps 2016 Conference*, SpaceOps Conferences, <https://doi.org/10.2514/6.2016-2481> (American Institute of Aeronautics and Astronautics, 2016).
11. Ruszczak, B. *et al.* Machine learning detects anomalies in OPS-SAT telemetry. In Mikyška, J. *et al.* (eds.) *Computational Science – ICCS 2023*, 295–306, https://doi.org/10.1007/978-3-031-35995-8_21 (Springer Nature Switzerland, Cham, 2023).
12. Kapoor, S. & Narayanan, A. Leakage and the reproducibility crisis in machine-learning-based science. *Patterns* **4**, 100804, <https://doi.org/10.1016/j.patter.2023.100804> (2023).
13. Ruszczak, B., Kotowski, K., Nalepa, J. & Evans, D. OPSSAT-AD - anomaly detection dataset for satellite telemetry, <https://doi.org/10.5281/zenodo.12588359> (2024).
14. Shendy, R. & Nalepa, J. Few-shot satellite image classification for bringing deep learning on board OPS-SAT. *Expert. Syst. with Appl.* **251**, 123984, <https://doi.org/10.1016/j.eswa.2024.123984> (2024).

15. ESA. WebMUST - web client for OPS-SAT directory. <https://opssat1.esoc.esa.int/webclient-must> (2021).
16. Ruszczak, B., Kotowski, K., Andrzejewski, J., Haskamp, C. & Nalepa, J. Oxi: An online tool for visualization and annotation of satellite time series data. *SoftwareX* **23**, 101476, <https://doi.org/10.1016/j.softx.2023.101476> (2023).
17. Nalepa, J. *et al.* Toward on-board detection of anomalous events from OPS-SAT telemetry using deep learning. In *8th International Workshop On On-Board Payload Data Compression*, <https://doi.org/10.5281/zenodo.7244991> (Zenodo, 2022).
18. Nalepa, J. *et al.* Look ma, no ground truth! on building supervised anomaly detection from OPS-SAT telemetry. In *Proceedings of the International Astronautical Congress, 2023, International Astronautical Federation*, 1–8 (2023).
19. Zhang, J. *et al.* Feature interpolation convolution for point cloud analysis. *Comput. & Graph.* **99**, 182–191, <https://doi.org/10.1016/j.cag.2021.06.015> (2021).
20. Lubba, C. H. *et al.* catch22: CAnonical Time-series CHaracteristics. *Data Min. Knowl. Discov.* **33**, 1821–1852, [10.1007/s10618-019-00647-x](https://doi.org/10.1007/s10618-019-00647-x) (2019).
21. Tafazoli, S. *et al.* C22mp: the marriage of catch22 and the matrix profile creates a fast, efficient and interpretable anomaly detector. *Knowl. Inf. Syst.* <https://doi.org/10.1007/s10115-024-02107-5> (2024).
22. Baldi, P., Brunak, S., Chauvin, Y., Andersen, C. A. F. & Nielsen, H. Assessing the accuracy of prediction algorithms for classification: an overview. *Bioinformatics* **16**, 412–424, <https://doi.org/10.1093/bioinformatics/16.5.412> (2000). https://academic.oup.com/bioinformatics/article-pdf/16/5/412/48836094/bioinformatics_16_5_412.pdf.
23. Grüning, M. & Kropf, S. A ridge classification method for high-dimensional observations. In Spiliopoulou, M., Kruse, R., Borgelt, C., Nürnberger, A. & Gaul, W. (eds.) *From Data and Information Analysis to Knowledge Engineering*, 684–691, https://doi.org/10.1007/3-540-31314-1_84 (Springer Berlin Heidelberg, Berlin, Heidelberg, 2006).
24. Fan, R.-E., Chang, K.-W., Hsieh, C.-J., Wang, X.-R. & Lin, C.-J. Liblinear: A library for large linear classification. *J. Mach. Learn. Res.* **9**, 1871–1874 (2008).
25. Hastie, T. J., Rosset, S., Zhu, J. & Zou, H. Multi-class adaboost. *Stat. Its Interface* **2**, 349–360, <https://doi.org/10.4310/SII.2009.v2.n3.a8> (2009).
26. Lee, C.-P. & Lin, C.-J. A study on l2-loss (squared hinge-loss) multiclass SVM. *Neural Comput.* **25**, 1302–1323, https://doi.org/10.1162/NECO_a_00434 (2013).
27. Zhao, Y. & Hryniewicki, M. K. Xgbod: Improving supervised outlier detection with unsupervised representation learning. In *2018 International Joint Conference on Neural Networks (IJCNN)*, 1–8, <https://doi.org/10.1109/IJCNN.2018.8489605> (2018).
28. Kwon, D. *et al.* A survey of deep learning-based network anomaly detection. *Clust. Comput.* **22**, 949–961, <https://doi.org/10.1007/s10586-017-1117-8> (2019).
29. Mastrangelo, C. M., Runger, G. C. & Montgomery, D. C. Statistical process monitoring with principal components. *Qual. Reliab. Eng. Int.* **12**, 203–210, [https://doi.org/10.1002/\(SICI\)1099-1638\(199605\)12:3<203::AID-QRE12>3.0.CO;2-B](https://doi.org/10.1002/(SICI)1099-1638(199605)12:3<203::AID-QRE12>3.0.CO;2-B) (1996).
30. Aggarwal, C. C. *Linear Models for Outlier Detection*, 65–110 (Springer International Publishing, Cham, 2017).
31. Arning, A., Agrawal, R. & Raghavan, P. A linear method for deviation detection in large databases. In *Knowledge Discovery and Data Mining*, vol. 1141, 972–981 (1996).
32. Tang, J., Chen, Z., Fu, A. W.-c. & Cheung, D. W. Enhancing effectiveness of outlier detections for low density patterns. In Chen, M.-S., Yu, P. S. & Liu, B. (eds.) *Advances in Knowledge Discovery and Data Mining*, 535–548 (Springer Berlin Heidelberg, Berlin, Heidelberg, 2002).
33. Angiulli, F. & Pizzuti, C. Fast outlier detection in high dimensional spaces. In Elomaa, T., Mannila, H. & Toivonen, H. (eds.) *Principles of Data Mining and Knowledge Discovery*, 15–27, https://doi.org/10.1007/3-540-45681-3_2 (Springer Berlin Heidelberg, Berlin, Heidelberg, 2002).
34. He, Z., Xu, X. & Deng, S. Discovering cluster-based local outliers. *Pattern Recognit. Lett.* **24**, 1641–1650, [https://doi.org/10.1016/S0167-8655\(03\)00003-5](https://doi.org/10.1016/S0167-8655(03)00003-5) (2003).
35. Kriegel, H.-P., Schubert, M. & Zimek, A. Angle-based outlier detection in high-dimensional data. In *Proceedings of the 14th ACM SIGKDD International Conference on Knowledge Discovery and Data Mining, KDD '08*, 444–452, <https://doi.org/10.1145/1401890.1401946> (Association for Computing Machinery, New York, NY, USA, 2008).

36. Liu, F. T., Ting, K. M. & Zhou, Z.-H. Isolation forest. In *2008 Eighth IEEE International Conference on Data Mining*, 413–422, <https://doi.org/10.1109/ICDM.2008.17> (2008).
37. Kriegel, H.-P., Kröger, P., Schubert, E. & Zimek, A. Outlier detection in axis-parallel subspaces of high dimensional data. In Theeramunkong, T., Kijssirikul, B., Cercone, N. & Ho, T.-B. (eds.) *Advances in Knowledge Discovery and Data Mining*, 831–838 (Springer Berlin Heidelberg, Berlin, Heidelberg, 2009).
38. Janssens, J. H. M., Huszár, F., Postma, E. O. & van den Herik, H. J. Stochastic outlier selection. Tech. Rep. TiCC TR 2012-001, Tilburg University, Center for Cognition and Communication, Tilburg, The Netherlands (2012).
39. Kingma, D. P. & Welling, M. Auto-encoding variational bayes. *CoRR* **abs/1312.6114** (2013).
40. Erfani, S. M., Rajasegarar, S., Karunasekera, S. & Leckie, C. High-dimensional and large-scale anomaly detection using a linear one-class SVM with deep learning. *Pattern Recognit.* **58**, 121–134, <https://doi.org/10.1016/j.patcog.2016.03.028> (2016).
41. Pevný, T. Loda: Lightweight on-line detector of anomalies. *Mach. Learn.* **102**, 275–304, <https://doi.org/10.1007/s10994-015-5521-0> (2016).
42. Schlegl, T., Seeböck, P., Waldstein, S. M., Schmidt-Erfurth, U. & Langs, G. Unsupervised anomaly detection with generative adversarial networks to guide marker discovery. In Niethammer, M. *et al.* (eds.) *Information Processing in Medical Imaging*, 146–157 (Springer International Publishing, Cham, 2017).
43. Ruff, L. *et al.* Deep one-class classification. In Dy, J. & Krause, A. (eds.) *Proceedings of the 35th International Conference on Machine Learning*, vol. 80 of *Proceedings of Machine Learning Research*, 4393–4402 (PMLR, 2018).
44. Zenati, H., Romain, M., Foo, C.-S., Lecouat, B. & Chandrasekhar, V. Adversarially learned anomaly detection. In *2018 IEEE International Conference on Data Mining (ICDM)*, 727–736, <https://doi.org/10.1109/ICDM.2018.00088> (2018).
45. Bandaragoda, T. R. *et al.* Isolation-based anomaly detection using nearest-neighbor ensembles. *Comput. Intell.* **34**, 968–998, <https://doi.org/10.1111/coin.12156> (2018).
46. Liu, Y. *et al.* Generative adversarial active learning for unsupervised outlier detection. *IEEE Transactions on Knowl. Data Eng.* **32**, 1517–1528, <https://doi.org/10.1109/TKDE.2019.2905606> (2020).
47. Li, Z., Zhao, Y., Botta, N., Ionescu, C. & Hu, X. Copod: Copula-based outlier detection. *2020 IEEE Int. Conf. on Data Min. (ICDM)* 1118–1123 (2020).
48. Li, Z. *et al.* ECOD: Unsupervised outlier detection using empirical cumulative distribution functions. *IEEE Trans. on Knowl. Data Eng.* **35**, 12181–12193, <https://doi.org/10.1109/TKDE.2022.3159580> (2022).
49. Goodge, A., Hooi, B., Ng, S.-K. & Ng, W. S. Lunar: Unifying local outlier detection methods via graph neural networks. *Proc. AAAI Conf. on Artif. Intell.* **36**, 6737–6745, <https://doi.org/10.1609/aaai.v36i6.20629> (2022).
50. Xu, H., Pang, G., Wang, Y. & Wang, Y. Deep isolation forest for anomaly detection. *IEEE Transactions on Knowl. Data Eng.* **35**, 12591–12604, <https://doi.org/10.1109/TKDE.2023.3270293> (2023).
51. Zhao, Y., Nasrullah, Z. & Li, Z. PyOD: A Python Toolbox for Scalable Outlier Detection. *J. Mach. Learn. Res.* **20**, 1–7 (2019).
52. Zhao, Y., Nasrullah, Z. & Li, Z. PyOD: A python toolbox for scalable outlier detection. *J. Mach. Learn. Res.* **20**, 1–7 (2019).
53. Abadi, M. *et al.* TensorFlow: Large-scale machine learning on heterogeneous systems (2015). Software available from tensorflow.org.
54. Paszke, A. *et al.* Automatic differentiation in pytorch (2017).
55. Harris, C. R. *et al.* Array programming with NumPy. *Nature* **585**, 357–362, <https://doi.org/10.1038/s41586-020-2649-2> (2020).
56. The Pandas development team. pandas-dev/pandas: Pandas, <https://doi.org/10.5281/zenodo.3509134> (2020).
57. Waskom, M. L. Seaborn: statistical data visualization. *J. Open Source Softw.* **6**, 3021, <https://doi.org/10.21105/joss.03021> (2021).

Acknowledgements

This work was partially supported through the following projects: “On-board Anomaly detection from the OPS-SAT telemetry using deep learning” (40001373339/22/NL/GLC/ov) and “Few-shot anomaly detection in satellite telemetry” (4000141301) funded by the European Space Agency. JN was supported by the Silesian University of Technology grant for maintaining and developing research potential.

Author contributions statement

B.R., K.K. and J.N. conceived and designed the study. B.R. and D.E. acquired the data and performed the experiments. B.R. implemented the computational pipeline and performed the analyses. B.R. drafted the manuscript. K.K. and J.N. edited and improved the manuscript. D.E. revised the manuscript. All authors have read and approved the final manuscript.

Corresponding author

Correspondence to [Bogdan Ruszczak](#).

Competing interests

The authors declare no competing interests.

Supplementary Materials

The distribution of the extracted features elaborated for each telemetry segment included in our dataset is depicted in Figure 7. We compare the distribution for the training (\mathcal{T}) and test (Ψ) sets, to visualize the effect of the training-test dataset split on the feature distributions. Figure 8 provides a detailed view of the relations between the extracted features for the \mathcal{T} and Ψ sets. We rendered this plot to confirm that both subsets represent similar data distributions.

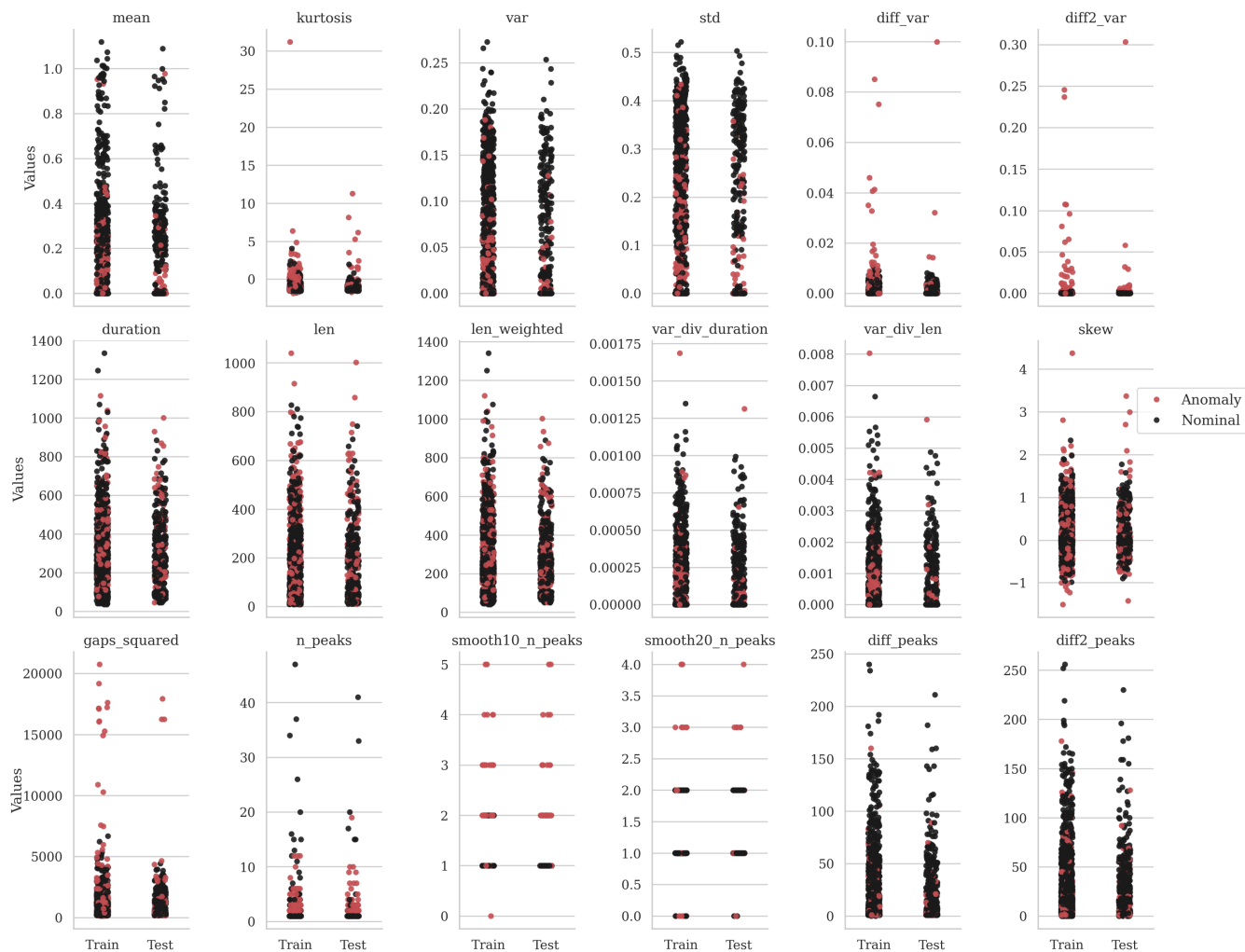


Figure 7. Dataset features for the training and validation subsets with the indication of anomalies (marked in red).

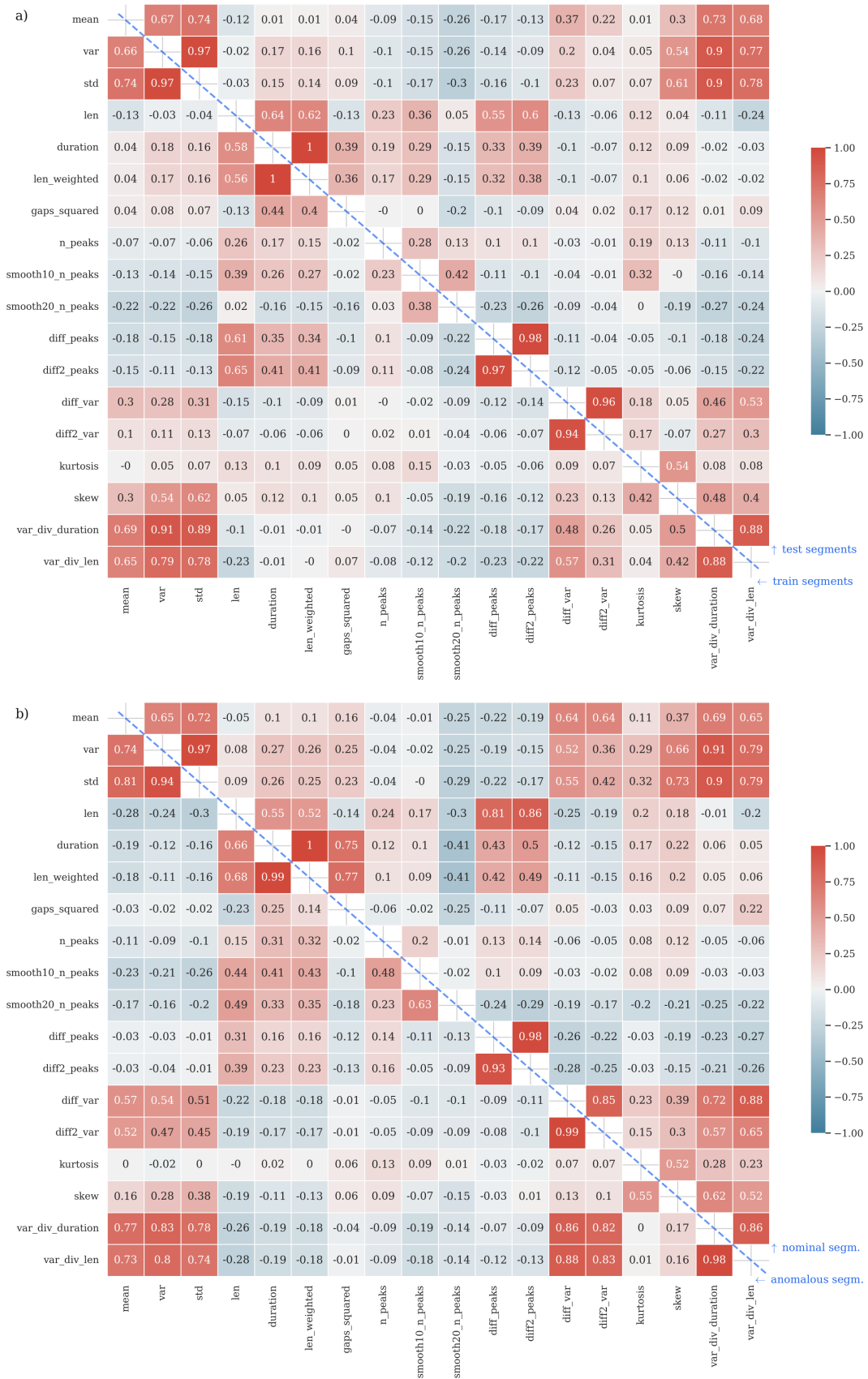


Figure 8. The coefficient of correlation computed between each feature, for the training (below the blue dashed diagonal line) and test set (above the same diagonal line). We employed: (a) Pearson's correlation coefficient and (b) Spearman's Rank correlation coefficient.